Ceramics International 43 (2017) 14347–14353

Contents lists available at ScienceDirect

Ceramics International

journal homepage: www.elsevier.com/locate/ceramint

Auto-ignition synthesis of $CoFe_2O_4$ with Al^{3+} substitution for high frequency applications

B.G. Toksha*, Sagar E. Shirsath, M.L. Mane, K.M. Jadhav

Department of Physics, Dr. Babasaheb Ambedkar Marathwada University, Aurangabad 431004, MS, India

ARTICLE INFO

Keywords:
Ferrites
Sol-gel auto combustion
Structural properties
Magnetization

ABSTRACT

A series of $CoAl_xFe_{2-x}O_4$ ($0 \le x \le 1.0$) was synthesized by sol-gel auto combustion method using nitrates of respective elements and by keeping 1:3 ratio of metal nitrate to citrate. The resultant powders were investigated by various techniques. Fourier transform infrared spectroscopy (FT-IR) is employed to determine the local symmetry in crystalline solids and to shed light on the ordering phenomenon. The XRD revealed that the powders obtained are single phase with inverse spinel structure. Evaluation of TEM confirms fine particle nature of the particles. SEM analysis and EDAX indicate that the samples were homogeneous and had the expected Fe-Co-Al ratios. As aluminium content increases, the measured magnetic hysteresis curves become broader and the saturation magnetization decreased. Coercivity increased from 975 to 4191 Oe with Al^{3+} substitution. An increase in electrical resistivity, coercivity and dielectric characterization made present samples suitable for use in high frequency device applications.

1. Introduction

The synthesis of spinel ferrite nanoparticles has been remained an issue of extensive study in recent years because of synthesis root have major role in deciding properties of product [1]. Magnetic nanoparticles produced through novel route along with their advantageous properties over bulk materials opens a new era of attractive possibilities in biomedical applications, such as magnetic hyperthermia, drug delivery, magnetic resonance imaging, and biosensors [2–4]. The heat generation that occurs in magnetic nanoparticles under external AC magnetic field has found applications in biomedicine. Cancer therapy by hyperthermia using magnetic nanoparticles, and drug targeting via thermo sensitive polymer conjugated magnetic nanoparticles had been focused as recent issues [5,6]. Permanent magnets of rare-earth (RE) based compounds are essential components in modern technologies, being employed in a huge number of large-scale and emerging applications, such as electronic devices, hard disks, automotive, wind turbines and hybrid – electric vehicles. The high environmental impact of mining, refining and recycling of RE compounds may represent a serious drawback for the economic sustainability of their massive exploitation. Therefore, the scientific community is looking for new RE-free materials.

Out of many ferrite compounds, $CoFe_2O_4$ has been the subject of research activities because of fundamental questions as well as potential application [7]. Ferrimagnetic $CoFe_2O_4$ exhibits excellent magnetic properties such as large magnetocrystalline anisotropy, high coercivity, and high saturation magnetization. Additionally, this material exhibits a significantly higher magnetostriction [8] and thus an excellent option to develop rare-earth free magnet. The search of a simple and economic route, which allows the preparation of a large amount of high-quality nanocrystalline $CoFe_2O_4$ is necessary and will benefit to practical applications of this interesting material with enhanced properties by doping [9].

Al substituted ferrite finds a wide range of applications at radio and microwave frequencies, where electrical and magnetic losses are required to be minimum [10–12]. The addition of Al^{3+} increases resistivity thereby lowering the dielectric losses and also decreases the saturation magnetization and alters the magnetic and electric properties of these materials [18]. These are properties suitable for manufacturing of micro-wave devices operating at L, S and C bands [15].

In this work we have introduced Al^{3+} ions as a replacement for Fe^{3+} ions in $CoFe_2O_4$ matrix and studied their structural, magnetic and dielectric variation for high frequency applications.

2. Synthesis

The nano-crystalline samples of the series $CoAl_xFe_{2-x}O_4$ were prepared by citrate nitrate sol-gel auto-ignition synthesis route. The A.R. grade citric acid ($C_6H_8O_7{\cdot}H_2O$), cobalt nitrate ($Co(NO_3)_2{\cdot}6H_2O$),

* Corresponding author.
E-mail address: mittoksha@gmail.com (B.G. Toksha).

http://dx.doi.org/10.1016/j.ceramint.2017.07.191
Received 17 July 2017; Received in revised form 26 July 2017; Accepted 27 July 2017
Available online 27 July 2017

aluminium nitrate($Al(NO_3)_3{\cdot}9H_2O$), ferric nitrate ($Fe(NO_3)_3{\cdot}9H_2O$) and ammonia (> 99% sd-fine) were used as starting materials.

In the present system, products were synthesized by keeping metal nitrates to citrate ratio 1:1 and adding ammonia maintaining pH at 6. The as-prepared powders of all the samples were heat treated separately at 500 °C for 4 h to get the final product. The as prepared and heat treated powders were used for further characterization.

The powder samples were examined by a Phillips X-ray diffractometer (Model 3710) using Cu Kα radiation (λ = 1.5405 Å). EDAX and scanning electron microscope (SEM) measurements were carried out on JEOL (Model JSM-840). Transmission electron microscope (TEM) measurements were recorded on Philips (Model CM 200). Fourier transform infrared spectroscopy (FTIR) measurements were carried out in the wave number range of 400–4000 cm^{-1} on Perkin-Elmer (Model V755). Magnetization measurements of the samples were carried out using a vibrating sample magnetometer (Make: Lakeshore, Model: 7307). The dielectric parameters were recorded on the Precision Impedance analyzer (Make: Agilent).

3. Results and discussion

3.1. Structural aspects

X-ray diffraction was performed on the as-burnt powders as well as on the 500 °C calcined powder. The X-ray powder diffraction patterns for all the compositions of as prepared $CoAl_xFe_{2-x}O_4$ were recorded and are shown in Fig. 1. The X-ray powder diffraction patterns for all the compositions of heat treated $CoAl_xFe_{2-x}O_4$ were recorded and are shown in Fig. 2. The reflection peaks of samples become sharper and narrower after the heat treatment at 500 °C, indicating the improvement of crystallinity and increase of the particle size.

The X-ray diffraction patterns show the formation of cubic spinel structure without appearance of any extra peaks representing secondary phases. All other peaks in the XRD pattern matches well with the characteristic reflections. The Interplaner spacing (d) values were calculated for the recorded peaks using Bragg's law and the lattice constant 'a' was calculated for each plane. The average lattice parameter 'a' may be obtained by calculating the average of the 'a' values for each diffraction plane [13]. It is found that the lattice parameter decreases with increasing Al ion substitution. The decrease of the value of the lattice parameter with increasing Al ion substitution can be explained on the basis of ionic radius, where the ionic radius of Al^{3+} ion (0.57 Å) is smaller than that of Fe^{3+} ion (0.67 Å). Theoretical lattice constant (a_{th}) was calculated using the equation discussed elsewhere [14] 'a_{th}' lie between 8.382 Å and 8.220 Å which agree with that of 'a' however the values of 'a_{th}' are little smaller than the values of 'a'. The bulk densities (ρ_{th}) of the specimens were about 90% of the corresponding X-ray density ($\rho_{x\text{-}ray}$). It is clear that the increase in composition x decreases $\rho_{x\text{-}ray}$. The X-ray density decreases with Al^{3+} concentration for all compositions, because the decrease in mass over takes the decrease in volume of the unit cell. The decrease in the bulk density is correlated with atomic weight of substituted Al^{3+} ions instead of Fe^{3+} ions. This decrease in bulk density may be due to the fact that Al^{3+} has smaller atomic weight (26.98 amu) than the Fe^{3+} (55.85 amu) atoms. It can be seen from the values that the prepared samples porosity ranges in 9–15%.

The particle size of all the samples was determined using Scherrer formula [15]. The highest intensity peak (311) of the XRD pattern is considered for the determination of fullwidth at half maxima (FWHM). It is evident from the particle size values that the particles are of nanosized nature.

The specific surface area of the prepared samples showed significant change with aluminium incorporation into the spinel cobalt ferrite

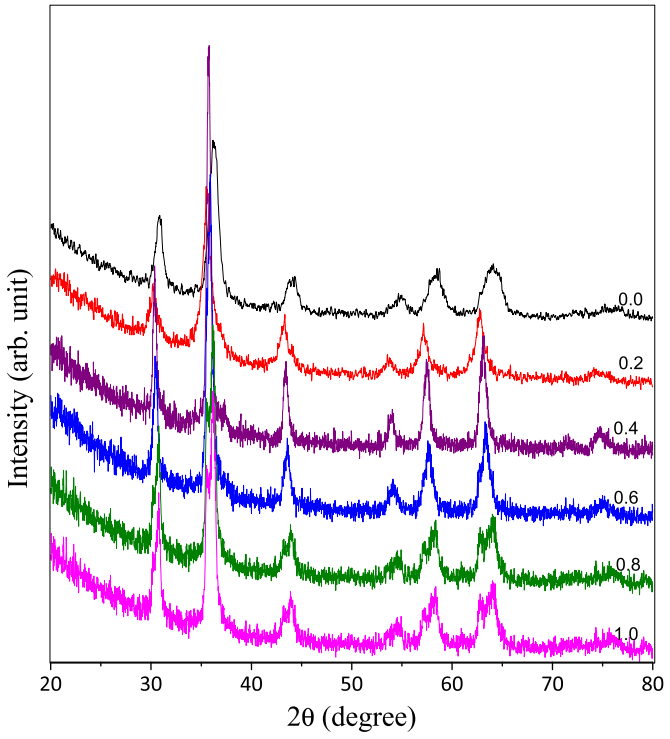

Fig. 1. XRD patterns of $CoAl_xFe_{2-x}O_4$ (as prepared).

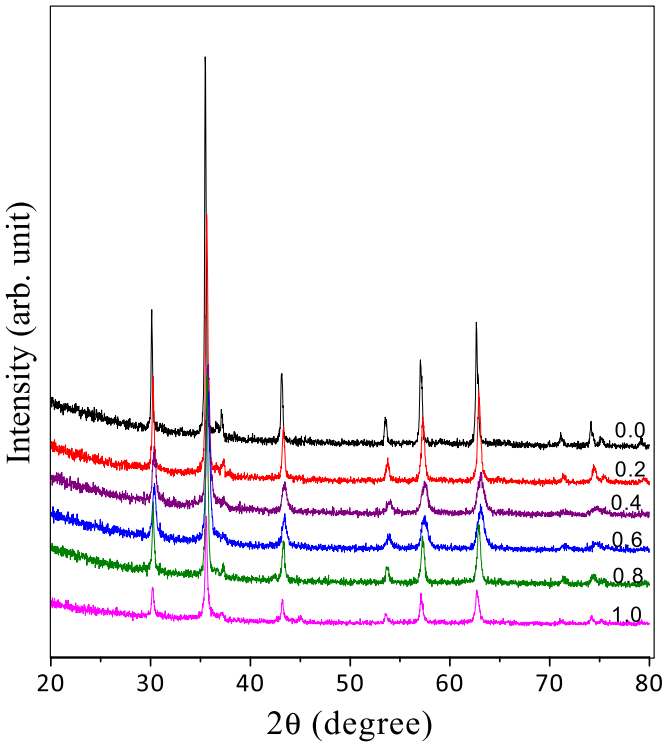

Fig. 2. XRD patterns of $CoAl_xFe_{2-x}O_4$ (500 °C heat treated).

Table 1
Stoichiometric % concentration of the constituent elements of the ferrite system $CoAl_xFe_{2-x}O_4$ by EDAX.

Composition x	Co	Fe	Al	O
0.0	14.72	29.17	0	56.11
0.6	14.17	23.67	5.98	56.18
1.0	14.17	15.07	14.6	56.16

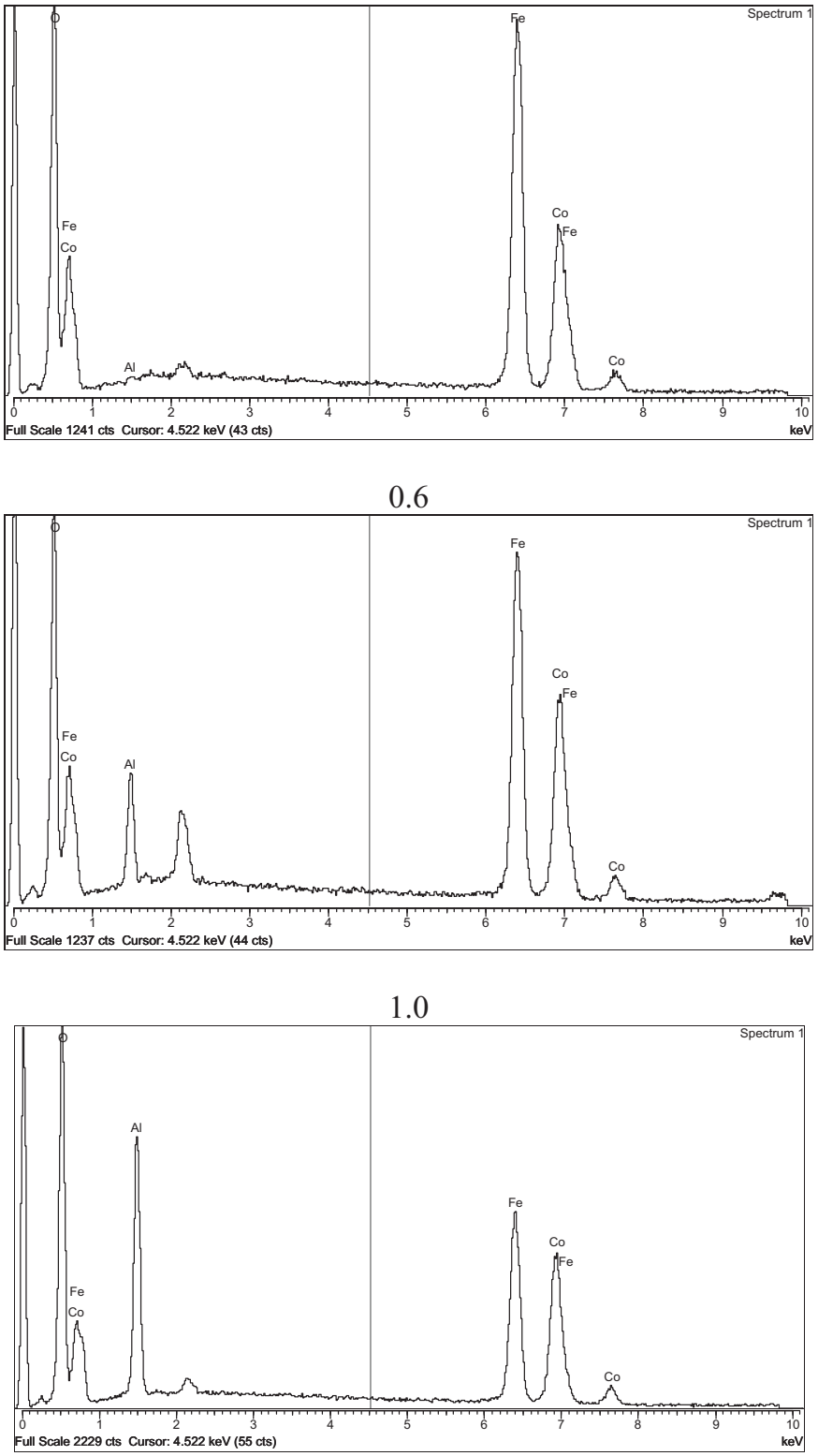

Fig. 3. EDAX of $CoAl_xFe_{2-x}O_4$ (0.2, 0.6 and 1.0).

structure. The specific surface area is found in the range of 47–160 m^2/g for as-prepared samples whereas it was in range of 21–120 m^2/g for heat treated samples.

Elemental analyses of the heat treated nanoparticles powder were performed at energy dispersive spectroscope equipped onto the SEM instrument. The % concentration of the constituent elements of the ferrite system $CoAl_xFe_{2-x}O_4$ is given in Table 1. It can be concluded from Table 1 that there is a little deviation from stoichiometry and constituent elements are in almost correct molar ratio. The energy dispersive spectrums of particular compositions are given Figs. 3 and 4 depicts the scanning electron microscope images for typical samples (x = 0.0, 0.6, 1.0). Morphologies of particles were observed by means of a

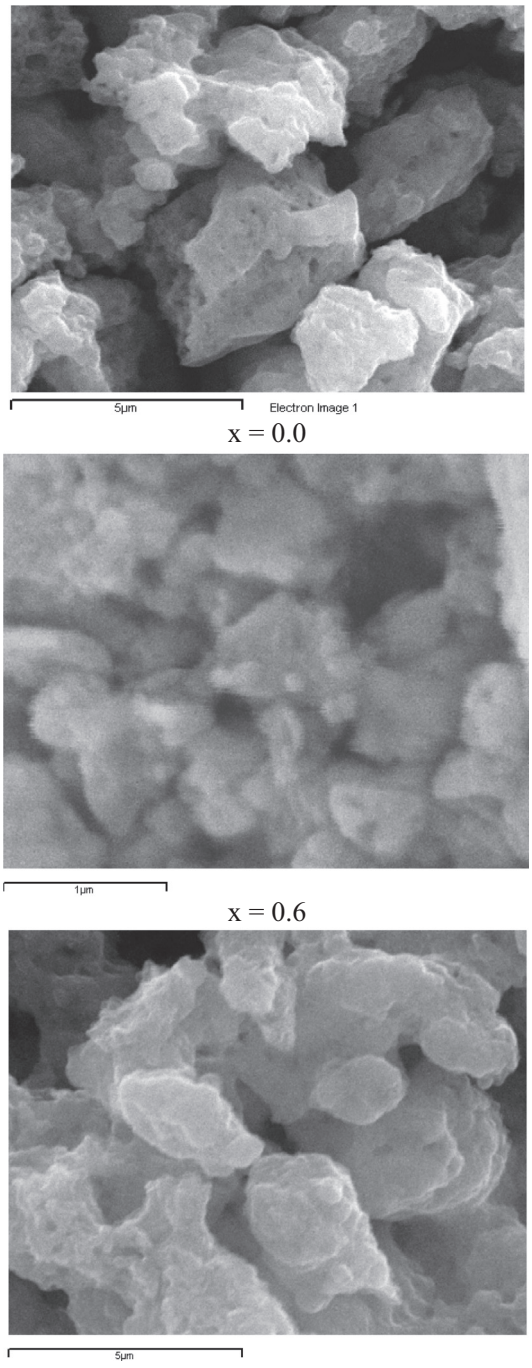

Fig. 4. SEM images of $CoAl_xFe_{2-x}O_4$ (x = 0.0, 0.6 and 1.0).

SEM image. SEM micrographs showed freely distributed sharp edged grains. Shapes of the grains are spherical or elliptical. The heat treated compound showed smaller size distribution.

Transmission electron microscopy was performed to observe the microstructure, particle size and morphology of the as prepared samples first and last composition. The TEM images of typical compositions (x = 0.0, 1.0) along with corresponding electron diffraction patterns are given in Fig. 5. The average particle size of the first composition from TEM image is found out to be 16 nm whereas for the last composition it came around 9 nm. Nanoparticles are all in an agglomerated state and have spherical shape. Diffused electron diffraction pattern is observed in case of as prepared samples of both the composition, which is indication of very less crystallinity and nano size of the synthesized particles.

3.2. Cation distribution

The electrical and magnetic properties of spinel ferrites are very sensitive to the arrangement of cations at available site, type, and amount of dopants. Therefore it was thought that it is essential to determine the cation distribution in $CoAl_xFe_{2-x}O_4$ system. Various methods are used to determine the cation distribution in a spinel ferrite. X-ray diffraction [16], Mössbauer spectroscopy [17], neutron diffraction [18], and magnetization [19] are the methods available to determine the cation distribution.

he cation distribution in $CoAl_xFe_{2-x}O_4$ ferrite system was calculated using R-factor method. In this method, the best structure is selected so that the value of residual function *R* is minimized. The intensities of planes which are mostly sensitive to cations on tetrahedral and octahedral sites are taken in to consideration while determining the cation distribution in the presently selected system. The ionic configuration based on the site preference energy value for individual cation suggested that Co^{2+}, Al^{3+} and Fe^{3+} ions can occupy both A- and B-sites [20]. Finally, the cation distribution is estimated for the best fit X-ray intensity ratio and listed in Table 2, which clearly shows that the Al^{3+} ions enter into A- and B-sites in the ~ 2:3 ratio. The presently calculated cation distribution is comparable to that reported in literature [21].

3.3. Infrared spectroscopy

Fourier transform infrared techniques were used to study the composition characteristics of the as-prepared sample. Fig. 6 represents the FTIR spectrum of the as-prepared powder particles in KBr for the composition x = 0.0, 0.4, and 1.0. Two absorption bands corresponding to the vibration of tetrahedral and octahedral complexes at around 600 and 400 cm^{-1} respectively can be observed in the FTIR spectrum. The bands with peaks observed at 1044.51 cm^{-1} and 1114.88 cm^{-1} can be assigned to O–H bending vibration [22]. The 1313.19, 1343.58 and 1383.56 cm^{-1} peaks are attributed to the characteristic–CH3 bending. The band observed between 1480 and 1700 cm^{-1} indicate the presence of nitro compounds [22,23]. The peaks at 2840.51 and 2920.47 cm^{-1} are due to C–H stretching vibration [22,23].

Infrared spectroscopy may be used to determine the local symmetry in crystalline solids and it also put light on the ordering phenomenon in the spinel structure [24]. The cubic spinel, with the space group $Fd_3mO^7_h$ has four infrared active vibrations. The substitution of different ions changes the parameters like the metal oxygen bond strength, the metal oxygen bond length and dimensions of the unit cell. All these parameters affect the infrared spectrum. Only two major bands were observed for all the compositions. The presence of third band could be observed. The first two bands ν_1 and ν_2 at around 600 cm^{-1} and 400 cm^{-1} respectively were attributed to the Fe^{3+}-O bonds on the tetrahedral A and octahedral B site respectively [25,26]. The shift of position of ν_1 and ν_2 bands towards higher side suggests occupancy of Al^{3+} at tetrahedral-A and octahedral B-site (Table 3). However, due to the substitution of Al^{3+} ions the broadening of ν_2 bonds takes place which may be due to the occupancy of cations of different characters on the same site [27]. The slight but distinct displacement of absorption band with increasing composition factor x indicates the increasing incorporation of Co ion at B-site. The ratio of the line positions of ν_1 and ν_2 is given by the relation [28]

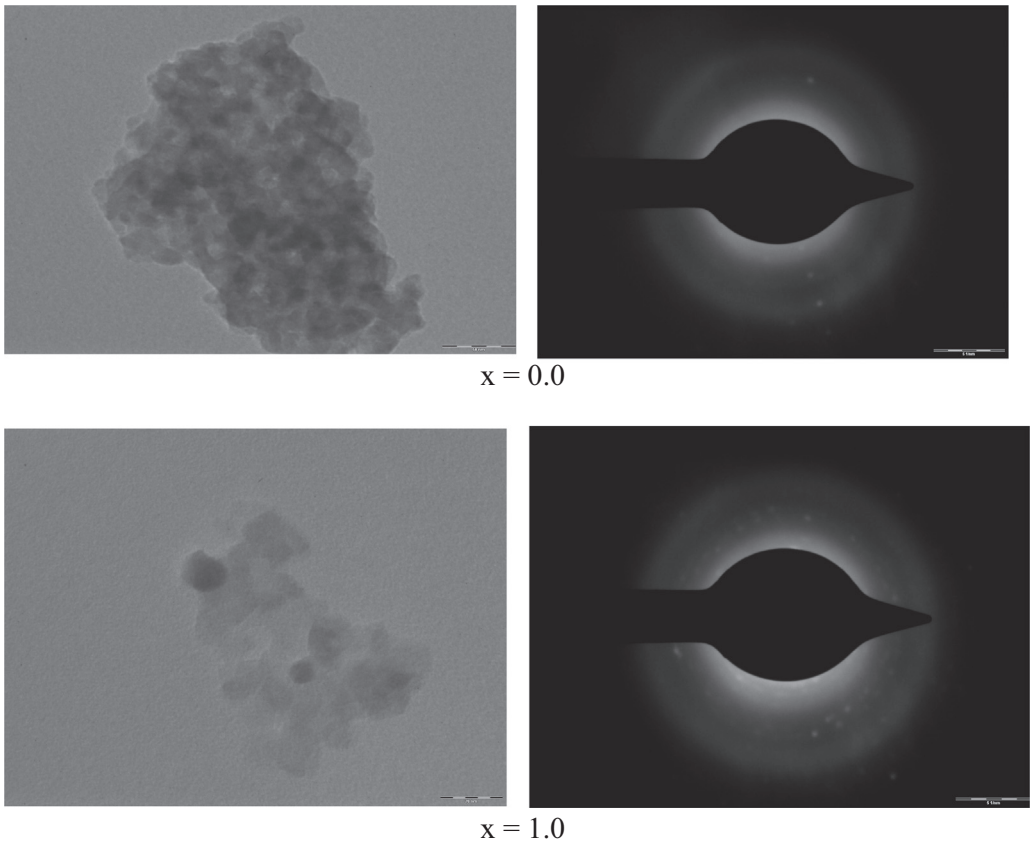

Fig. 5. TEM images of $CoAl_xFe_{2-x}O_4$ (x = 0.0 and 1.0).

Table 2
Cation distribution of the ferrite system $CoAl_xFe_{2-x}O_4$ system.

Composition	A site	B site
0.0	$Co_{0.25}Fe_{0.75}$	$Co_{0.75}Fe_{1.25}$
0.2	$Co_{0.21}Al_{0.04}Fe_{0.75}$	$Co_{0.79}Al_{0.16}Fe_{1.05}$
0.4	$Co_{0.18}Al_{0.12}Fe_{0.70}$	$Co_{0.82}Al_{0.28}Fe_{0.90}$
0.6	$Co_{0.20}Al_{0.20}Fe_{0.60}$	$Co_{0.80}Al_{0.40}Fe_{0.80}$
0.8	$Co_{0.10}Al_{0.30}Fe_{0.60}$	$Co_{0.90}Al_{0.50}Fe_{0.60}$
1.0	$Co_{0.10}Al_{0.35}Fe_{0.55}$	$Co_{0.90}Al_{0.65}Fe_{0.45}$

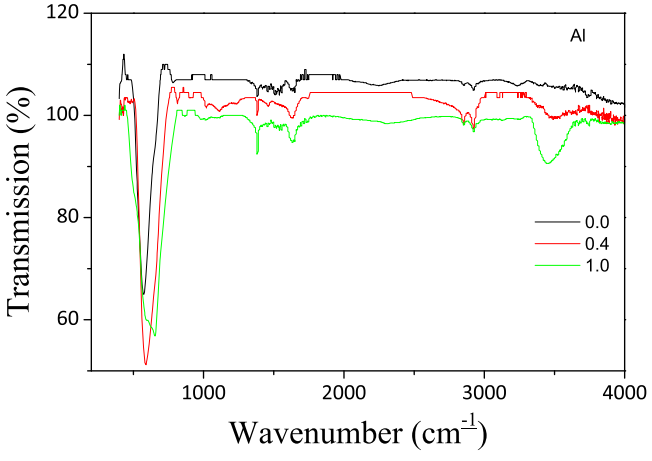

Fig. 6. FTIR patterns of $CoAl_xFe_{2-x}O_4$ (x = 0.0, 0.4 and 1.0).

Table 3
The infra red absorption bands (ν_1 and ν_2) and force constants (K_O and K_t) of the ferrite system $CoAl_xFe_{2-x}O_4$ system.

Composition	Absorption bands		Force constant	
	ν_1 cm^{-1}	ν_2 cm^{-1}	$K_0 \times 10^5$ (Dyne/cm^2)	$K_t \times 10^5$ (Dyne/cm^2)
0.0	584	403	0.978	1.684
0.2	586	405	0.979	1.681
0.4	589	408	0.977	1.675
0.6	590	410	0.971	1.660
0.8	590	410	0.946	1.619
1.0	593	413	0.948	1.616

$$\frac{\upsilon_1}{\upsilon_2} = \frac{K_T}{K_O}\sqrt{2}$$

Here, K_T and K_O designate the force constants associated with the unit displacement of a cation-oxygen in the tetrahedral (A) and octahedral (B) site, respectively. When this ratio deviates from unit it means that the expansion in the octahedral site is not equally compensated by the same amount of shrinkage of tetrahedral sites. IR spectra were also used to study the force constants for tetrahedral and octahedral sites. There values are listed in Table 3. It can be seen from the table that there is a small but gradual decrease in tetrahedral and octahedral force constants. This variation of force constant could be due to the decrease in the lattice parameter and bond lengths with the addition of Al in cobalt ferrite matrix.

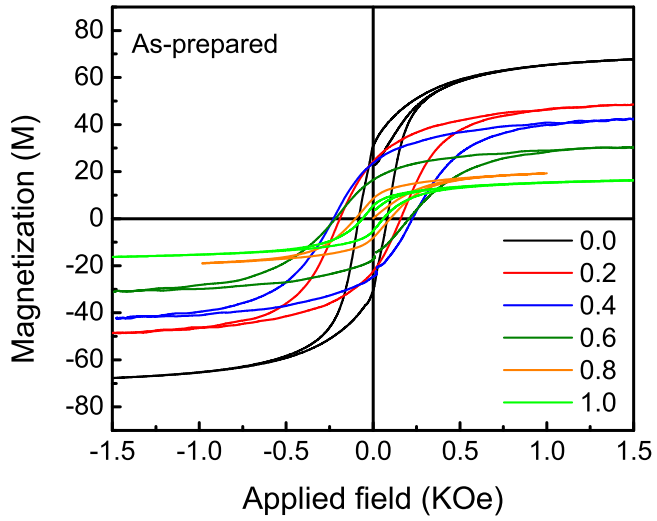

Fig. 7. Variation of magnetization (M) with applied magnetic field (H) for all the as-prepared samples of $CoAl_xFe_{2-x}O_4$.

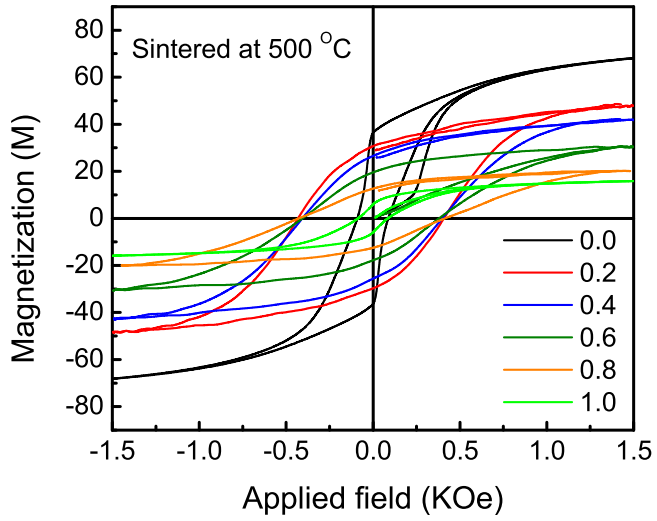

Fig. 8. Variation of magnetization (M) with applied magnetic field (H) for all the sintered at 500 °C samples of $CoAl_xFe_{2-x}O_4$.

Table 4
Saturation magnetization (***Ms***), remanant magnetization (***Mr***), coercivity (***Hc***) and remanence magnetization (***R***) measured at room temperature of the ferrite system $CoAl_xFe_{2-x}O_4$ system as prepared (***ap***) and samples heated at 500 °C.

x	Ms (emu/g)		Mr (emu/g)		Hc (Oe)		R	
	ap	500 °C	***ap***	500 °C	***ap***	500 °C	***ap***	500 °C
0.0	67.94	69.15	29.14	36.07	890	975	0.43	0.52
0.2	46.66	48.92	23.43	30.29	1832	4191	0.50	0.62
0.4	42.24	43.56	21.19	26.19	2365	4008	0.50	0.60
0.6	30.14	36.77	16.24	19.71	2162	3813	0.54	0.54
0.8	20.23	20.27	7.5	12.63	1032	4124	0.37	0.62
1.0	16.02	16.14	6.43	6.63	790	846	0.40	0.41

3.4. Magnetic and dielectric aspects

Fig. 7 gives the curve of magnetization versus applied field for all as prepared samples and for heat treated samples the magnetization curves were as shown in Fig. 8 of the present series $CoAl_xFe_{2-x}O_4$ (x = 0.0–1.0, in steps of 0.2). The magnetization curve reveals the change in magnetic behavior in the parent cobalt ferrite with aluminium substitution. The magnetization curves are used to get the values of saturation magnetization, remanant magnetization and coercivity. The values of saturation magnetization, remanant magnetization and coercivity are given in Table 4. It is observed that saturation magnetization decreased with aluminium substitution.

In the Neel's two sublattice collinear spin model, the magnetization depends on the cation distribution in the A and B site. The spins at both sites are coupled anti-ferromagnetically leading to the net magnetization per formula unit at 0 K (Ms) which is simply the numerical difference between sublattice magnetization. Keeping in mind the known magnetic moments for Al^{3+} (0 μB), Co^{2+} (3 μB), and Fe^{3+} (5 μB) the variation in saturation magnetization (M_S) with substituent concentration, x, can be explained. With substitution of Al^{3+}, the saturation magnetization (M_S) decreases. The introduction of aluminium ions in place of iron ions tetrahedral A and octahedral B sites dilutes both the A and B sub-lattices simultaneously. The net magnetization, being the difference between A and B sublattice magnetizations, is observed to decrease. The incorporation of aluminium ions into the A-sublattice and B-sublattice leads to larger decrease in magnetic moment of A-sublattice as compared to that of B-sub lattice so that the total magnetic moment

The remanant ratio R = Mr/Ms is a characteristic parameter of the material. High remanant ratio is desirable for magnetic recording and memory devices. It is an indication of the ease with which the direction of magnetization reorients to nearest easy axis magnetization direction after the magnetic field is removed. The lower value of remanant ratio is indication of isotropic nature of material. It is observed that the values of R in the present case are in the range of 0.41–0.62 and shows random nature with Al^{3+} substitution. It is clearly observed from Table 4 that the coercivity (H_C) show significant enhancement upon Al^{3+} substitution for the samples sintered at 500 °C. The Hc is basically starts from 975 Oe (x = 0.0) and attains a maximum value of 4191 Oe (x = 0.02). This significant increase in coercivity and remanence magnetization refer to enhance magnetic hardening of $CoFe_2O_4$ upon Al^{3+} substitution.

The values of theoretical Neel's magnetic moment were calculated by considering the magnetic moments of constituent ions. It is observed that the experimental values are in good agreement with the calculated results. The magnetic moment supposed to decrease as the non magnetic aluminium content increases; this can be explained on the basis of magnetic moment of constituent ions. When x amount of aluminium are added, the percent Fe^{3+} ions are comparatively decreased from B-site by an larger amount as compared to A-site. Hence the addition of aluminium ions decreases the difference between A and B sub lattices magnetic moment.

High DC electrical resistivity is a pre-requisite for applying ferrites at high frequency applications to counter the eddy current losses, which degrade the ferrite performance. DC electrical resistivity for all the samples was measured by the two probe method as a function of composition. The measured values of DC electrical resistivity at 373 K were found to vary from 5.7×10^7 to 9.2×10^7 Ω cm as the concentration of Al^{3+} increases from x = 0.0–1.0.

The dielectric parameters such as dielectric constant (ε'), dielectric loss tangent (tan δ) of the samples were recorded as a function of Al^{3+} concentration at room temperature. The dielectric constant has been found to be 370 for x = 0.0 and reduced with the Al^{3+} up to 50 for x = 1.0 composition at a fixed frequency 5 MHz. The dielectric loss has been found less than 2.5 for x = 0.0 and reduced with the Al^{3+} up to 1.25 for x = 1.0 composition. The cation distribution plays the key role in understanding such behavior of decrease in dielectric parameters with increase in the Al^{3+} concentration. The addition of Al^{3+} results in

Table 5
Coercivity (*Hc*), remanant magnetization (*Mr*), and Dielectric constant (ε`) measured at room temperature of the ferrite system $CoAl_xFe_{2-x}O_4$ compared with literature values.

Composition	Hc (Oe)		Mr (emu/g)		Dielectric constant (ε`)	
	Present results	Literature value [30]	Present results	Literature value [30]	Present results	Literature value
0.0	975	1362	36.07	28.5	370	240 [31]
0.2	4191	1305	30.3	26.9	300	42 [32]
0.4	4008	1191	26.2	21.1	260	27 [32]
0.6	3813	1108	19.7	17.4	–	–
0.8	4124	868	12.6	12.4	–	–
1.0	846	856	6.6	5.4	50	–

the migration of Fe^{3+} ions from octahedral site to tetrahedral site, thereby decreasing the number of Fe^{3+}/Fe^{2+} [29]. Table 5 presents comparison of the results of the present work with that obtained in the literature for same compositions [30]. The literature values of the composition at which the dielectric constant values are recorded are slight varying with present work [31,32].

4. Conclusions

Al^{3+} substituted $CoFe_2O_4$ ferrites nanoparticles were synthesized via the sol-gel auto-ignition method. XRD and IR study reveals that the system prepared by solgel method technique has been single phased cubic spinel structure. The structural characterization of the powders using XRD and TEM confirmed the formation of nanosize particles. The occupation of Fe^{3+} ions decreases in the B- site as the introduction of Al^{3+} ions in the B- site increases. The distribution of the magnetic Fe^{3+} ions thus affected by Al^{3+} substitution has interesting effects on magnetic structure. Reduction of magnetization with increase of aluminium content is caused by non-magnetic Al^{3+} ions and weakened interaction between sublattices. Most importantly coercivity and remanent magnetization of $CoFe_2O_4$ ferrites shows remarkable enhancement with Al^{3+} substitution. The dielectric constant and dielectric loss has been found to reduce with increase in Aluminium concentration with very high values of resistivity, which makes synthesized material a good choice for high frequency applications.

References

[1] B.G. Toksha, S.E. Shirsath, M.L. Mane, S.M. Patange, S.S. Jadhav, K.M. Jadhav, Autocombustion high-temperature synthesis, structural, and magnetic properties of $CoCr_xFe_{2-x}O_4$, J. Phys. Chem. C 115 (2011) 20905–20912.

[2] B.G. Toksha, S.E. Shirsath, S.M. Patange, K.M. Jadhav, Structural investigations and magnetic properties of cobalt ferrite nanoparticles prepared by sol–gel auto combustion method, Solid State Commun. 147 (2008) 479–483.

[3] T. Hyeon, S.S. Lee, J.G. Park, Y. Chung, H.B. Na, Synthesis of highly crystalline and monodisperse maghemite nanocrystallites without a size-selection process, J. Am. Chem. Soc. 123 (2001) 12798.

[4] J. Park, K. An, Y. Hwang, J.G. Park, H.J. Noh, J.Y. Kim, J.H. Park, N.M. Hwang, T. Hyeon, Ultra-large-scale syntheses of monodisperse nanocrystals, Nat. Mater. 3 (2004) 891.

[5] A.P. Alivisatos, Semiconductor clusters, nanocrystals, and quantum dots, Science 271 (1996) 933.

[6] M. M-Almazo, S. G-Gutierrez, X. Gao, J.L. Elechiguerra, V.A. Kusuma, W.M. Sampson, M. M-Yoshida, A.B. Dalton, R. Escudero, M.J. Yacaman, Cobalt-based superparamagnetic nanorings, Nano Lett. 4 (2004) 1365.

[7] R. Sato Turtelli, Giap V. Duong, W. Nunes, R. Grossinger, M. Knobel, Magnetic properties of nanocrystalline CoFe2O4 synthesized by modified citrate-gel method, J. Magn. Magn. Mater. 320 (2008) e339.

[8] Sagar E. Shirsath, Xiaoxi Liu, Yukiko Yasukawa, Sean Li, Akimitsu Morisako, Switching of magnetic easy-axis using crystal orientation for large perpendicular coercivity in CoFe2O4 thin film, Sci. Rep. 6 (2016) 30074. http://dx.doi.org/10.1038/srep30074.

[9] Alberto López-Ortega, Elisabetta Lottini, César de Julián Fernández, Claudio Sangregorio, Exploring the magnetic properties of cobalt-ferrite nanoparticles for the development of a rare-earth-free permanent magnet, Chem. Mater. 27 (2015) 4048–4056.

[10] D.R. Mane, U.N. Devatwal, K.M. Jadhav, Structural and magnetic properties of aluminium and chromium co-substituted cobalt ferrite, Mater. Lett. 44 (2) (2000) 91–95.

[11] M. Mozaffari, J. Amighin, Preparation of Al-substituted Ni ferrite powders via mechanochemical processing, J. Magn. Magn. Mater. 260 (2003) 244.

[12] S. Rashonlel, N.D. Sharma, S.P. Taneja, A. Gupta, Mössbauer, X-ray and magnetization studies of $Ni_{0.5}Zn_{0.5}Al_xFe_{2-x}O_4$ system, Ind. J. Pure Appl. Phys. 43 (2005) 44.

[13] B.D. Cullity, Elements of X-ray Diffraction, Addison-Wesley, Reading, MA, 1956.

[14] S.M. Patange, Sagar E. Shirsath, B.G. Toksha, Santosh S. Jadhav, S.J. Shukla, K.M. Jadhav, Rietveld structure refinement, cation distribution and magnetic properties of Al^{3+} substituted $NiFe_2O_4$ nanoparticles, Appl. Phys. A: Mater. Sci. Process. A95 (2009) 429.

[15] Sagar E. Shirsath, B.G. Toksha, K.M. Jadhav, Structural and magnetic properties of In^{3+} substituted $NiFe_2O_4$, Mater. Chem. Phys. 117 (2009) 163.

[16] C.O. Arean, J.L.R. Blanco, J.M.R. Gonzalez, M.C.T. Fernandez, Structural characterization of polycrystalline gallium-substituted cobalt ferrites, J. Mater. Sci. Lett. 9 (1990) 229.

[17] V.K. Mittal, P. Chandramohan, Santanu Bera, M.P. Srinivasan, S. Velmurugan, S.V. Narasimhan, Cation distribution in NixMg1−xFe2O4 studied by XPS and Mössbauer spectroscopy, Solid State Commun. 137 (2006) 6.

[18] J.A. Gomes, M.H. Sousa, F.A. Tourinho, J. Mestnik-Filho, R. Itri, J. Depeyro, Rietveld structure refinement of the cation distribution in ferrite fine particles studied by X-ray powder diffraction, J. Magn. Magn. Mater. 289 (2005) 184.

[19] H. Furuhashi, M. Inagaki, S. Naka, Cation distribution in the solid solutions of the CoAl2O4, GeCo2O4 system, J. Inorg. Nucl. Chem. 35 (1973) 3009.

[20] J.B. Good Enough, A.L. Loeb, Theory of ionic ordering, crystal distortion, and magnetic exchange due to covalent forces in spinels, Phys. Rev. 98 (1953) 391.

[21] S. Singhal, S.K. Barthwal, K. Chandra, XRD, magnetic and Mössbauer spectral studies of nano size aluminum substituted cobalt ferrites (CoAlxFe2−xO4), J. Magn. Magn. Mater. 306 (2006) 233.

[22] C. Juliena, M.A. Camacho-Lopez, T. Mohan, S. Chitra, P. Kalyani, S. Gopukumar, Combustion synthesis and characterization of substituted lithium cobalt oxides in lithium batteries, Solid State Ion. 135 (2000) 241.

[23] L. Zhao, H. Zhang, Y. Xing, S. Song, S. Yua, W. Shia, X. Guo, J. Yang, Y. Lei, F. Cao, Studies on the magnetism of cobalt ferrite nanocrystals synthesized by hydrothermal method, J. Solid State Chem. 181 (2008) 245.

[24] S.M. Patange, S.E. Shirsath, B.G. Toksha, S.S. Jadhav, K.M. Jadhav, Electrical and magnetic properties of Cr^{3+} substituted nanocrystalline nickel ferrite, J. Appl. Phys. 106 (2009) (023914-1).

[25] B.K. Labde, Madan C. Sable, N.R. Shamkuwar, Structural and infra-red studies of Ni1+xPbxFe2−2xO4 system, Mater. Lett. 57 (2003) 1651.

[26] K.B. Modi, M.C. Chhantbar, H.H. Joshi, Study of elastic behaviour of magnesium ferri aluminates, Ceram. Int. 32 (2006) 111.

[27] S.A. Mazen, S.F. Mansoura, E. Dhahrib, H.M. Zakia, T.A. Elmosalamia, The conduction mechanism of Li–Ga ferrite, J. Alloy. Compd. 472 (2009) 307.

[28] I.H. Gul, A. Maqsood, Structural, magnetic and electrical properties of cobalt ferrites prepared by the sol–gel route, J. Alloy. Compd. 465 (2008) 227.

[29] M. Abdullah Dara, Khalid Mujasam Batoob, Vivek Vermac, W.A. Siddiquia, R.K. Kotnala, Synthesis and characterization of nano-sized pure and Al-doped lithium ferrite having high value of dielectric constant, J. Alloy. Compd. 493 (2010) 553.

[30] A.T. Raghavender, R.G. Kulkarni, K.M. Jadhav, Magnetic properties of mixed cobalt-aluminum ferrite nanoparticles, Chin. J. Phys. 48 (4) (2010) 512.

[31] S.M. Patange, K.S. Lohar, Sagar E. Shrisath, B.G. Toksha, S.S. Jadhav, N. Kulkarni, K.M. Jadhav, The effect of oxidizing agents on the electrical properties of cobalt ferrite, Phys. Scr. 82 (2010) (045703)(4pp).

[32] I.H. Gul, A. Maqsood, M. Naeem, M. Naeem Ashiq, Optical, magnetic and electrical investigation of cobalt ferrite nanoparticles synthesized by co-precipitation route, J. Alloy. Compd. 507 (2010) 201–206.